Assessment of Moisture Content of Fine-Grained Soils from Multispectral Imagery

J. Paprocki[1], N. Stark[2]
Charles E. Via, Jr. Department of Civil and Environmental Engineering, Virginia Tech, Blacksburg, USA, paprocja@vt.edu[1], ninas@vt.edu[2]

H. C. Graber
Center for Southeastern Tropical Advanced Remote Sensing, University of Miami, Miami, USA, hgraber@rsmas.miami.edu

ABSTRACT: A method for estimating the moisture content of bare, fine-grained soils from satellite-based multispectral imagery was tested. The moisture contents of two soils (one silt, one clay) at two sites (K1 and K8) at Kentland Farm near Blacksburg, USA were estimated based on reflectance values extracted from band 7 of the WorldView-2 satellite (770-895 nm). The calibration factors necessary for calculating moisture content were determined using laboratory-based spectrometer measurements. Field measurements of moisture content from soil samples for site K1 ranged between 11.8%-26.0% and between 7.7%-18.6% for K8. The estimated moisture contents ranged from 12.6%-22.4% for K1 and from 10.2%-19.9% for K8. Thus, the estimates of moisture content matched standard test methods, suggesting a promising pathway for estimating moisture contents of fine-grained soils from satellite imagery.

Keywords: moisture content; remote sensing; satellite image; reflectance; spectrometer

1. Introduction

Moisture content influences the strength of soils [1]. Coastal environments are typically characterized by one dominant mineralogical composition, loose sediments, and limited variability in grain size [2]. In these environments, moisture content is a key variable changing on a spatiotemporal scale and affecting soil strength [3, 4], and thus, issues such as beach trafficability [5, 6, 7], coastal erosion, and other engineering applications. Moisture content can vastly change in response to storm surges, wave runup, and rainfall events [3,4]. This calls for a methodology for rapidly mapping moisture content on different spatiotemporal scales.

Mapping moisture content from satellite-based multispectral imagery utilizes the reflectance, which represents the percentage of incident energy that is reflected off an object. Models for estimating moisture content utilizing reflectance data have been proposed in agricultural applications for a wide range of soil types [9-11] with applications in coastal environments generally tested only for sandy soils [12-16]. Reflectance data can either be obtained from ground-based spectrometers [9, 10, 13] or from aerial or satellite-based multispectral imagery [11, 12, 14, 15, 16]. These two methods, while similar, differ in how reflectance is assigned to wavelengths. Ground-based spectrometers operate over many narrow bands of wavelengths simultaneously, resulting in one reflectance value being assigned to each wavelength. The wavelengths over which data is collected spans many regions of the electromagnetic spectrum, ranging from the visible light spectrum (400 nm - 700 nm) into the infrared (IR) region (700 nm - 14000 nm). Satellite-based multispectral scanners also record reflectance values simultaneously over a range of wavelengths. However, these systems typically collect data over wider bands of wavelengths meaning that one average reflectance value is assigned to multiple wavelengths. Satellite-based multispectral sensors have multiple bands that typically fall within the visible or IR portions of the electromagnetic spectrum, with bands within the near-infrared (NIR) region (700 nm - 1300 nm) being the most common [17].

A simple exponential model put forth by Muller and Décamps [11] relates the moisture content of a soil to the reflectance of the soil in air dried conditions at a given wavelength ($\rho_{so(\lambda)}$, unitless), the reflectance of the soil at a given gravimetric moisture content (m, unitless), and an attenuation factor relating moisture content and the spectral reflectance at a given wavelength ($a_{s(\lambda)}$, unitless) in the form of Eq. (1):

$$\rho_{s(\lambda)} = \rho_{so(\lambda)} * e^{-a_{s(\lambda)} * m} \quad (1)$$

This model can be applied whether reflectance is found using ground-based or satellite-based measurements. However, Eq. (1) relies upon knowledge of the parameters $\rho_{so(\lambda)}$ and $a_{s(\lambda)}$, which vary depending upon the soil type and wavelengths over which the data is collected.

The parameter $\rho_{so(\lambda)}$ can be determined at sandy beaches with a sufficiently wide subaerial zone (i.e., higher elevation than the high tide) utilizing imagery data from this zone in comparison to wetter areas in the intertidal zone. Such zonation can often even be determined visually from digital images [3, 4, 14, 18]. However, these zones of dry material may not always exist, especially under extreme conditions such as heavy rainfall or surges. This drives the need to develop alternative methods for assessing the parameter $\rho_{so(\lambda)}$, such as from laboratory-based measurements of reflectance.

The parameter $a_{s(\lambda)}$ is calibrated using either satellite-based or ground-based spectrometers calibrated using ground-truth moisture content measurements conducted during the collection of reflectance data.

Most of the work for satellite imagery has focused on sandy soils. However, coastal environments are composed of a wide range of sediments [2], ranging from coarse-grained mixed sand and gravel beaches (for example, Advocate Beach in Nova Scotia, Canada) to fine-grained mudflats exposed during low tide (for example, Cook Inlet in Alaska, United States). For fine-grained sediments, it becomes more difficult to establish zones of dry soils in satellite imagery, especially when typical moisture content patterns of beaches are not present. Furthermore, it is also not always possible to obtain ground truth measurements of moisture content to calibrate satellite imagery for the necessary parameters.

Muller and Décamps [11] proposed that soils that have developed under similar geological processes can be modeled using the same value for $\rho_{so(\lambda)}$. The value of $a_{s(\lambda)}$ holds for a specific category of soils. Through literature review and online databases, it is then possible to establish a soil type and origin for a given site [8]. Then, it becomes feasible to establish reasonable values for $\rho_{so(\lambda)}$ and $a_{s(\lambda)}$ through laboratory-based spectrometer measurements of reflectance even for sites that cannot be accessed in the field.

The goal of this study is to test a method for estimating moisture content of two different fine-grained soils, a clay and a silt, with limited impacts due to vegetation and organic matter. Laboratory-based spectrometer measurements of reflectance are first used to establish the parameters $\rho_{so(\lambda)}$ and $a_{s(\lambda)}$. These parameters are then used to estimate the moisture content of fine-grained soils based on reflectance data obtained from satellite-based multispectral imagery.

2. Study Area

Kentland Farm of Virginia Tech (Fig. 1) is an agricultural research facility of about 7 km^2 and features a variety of soil types. Two different soils were selected for this study: a brown sandy silt (referred to as site K1) with a liquid limit of 36, a plastic limit of 31, and a black soil (referred to as site K8) that classifies on the border between a silt and lean clay with a liquid limit of 37, a plastic limit of 25. By size (using 2 μm as the division between silt and clay), K1 contained 60.2% silt, 5.0% clay, and 34.8 % sand, and K8 contained 71.4% silt, 20.0% clay, and 8.6% sand. Soil samples were classified following ASTM D2487 [19] and ASTM D6928 [20].

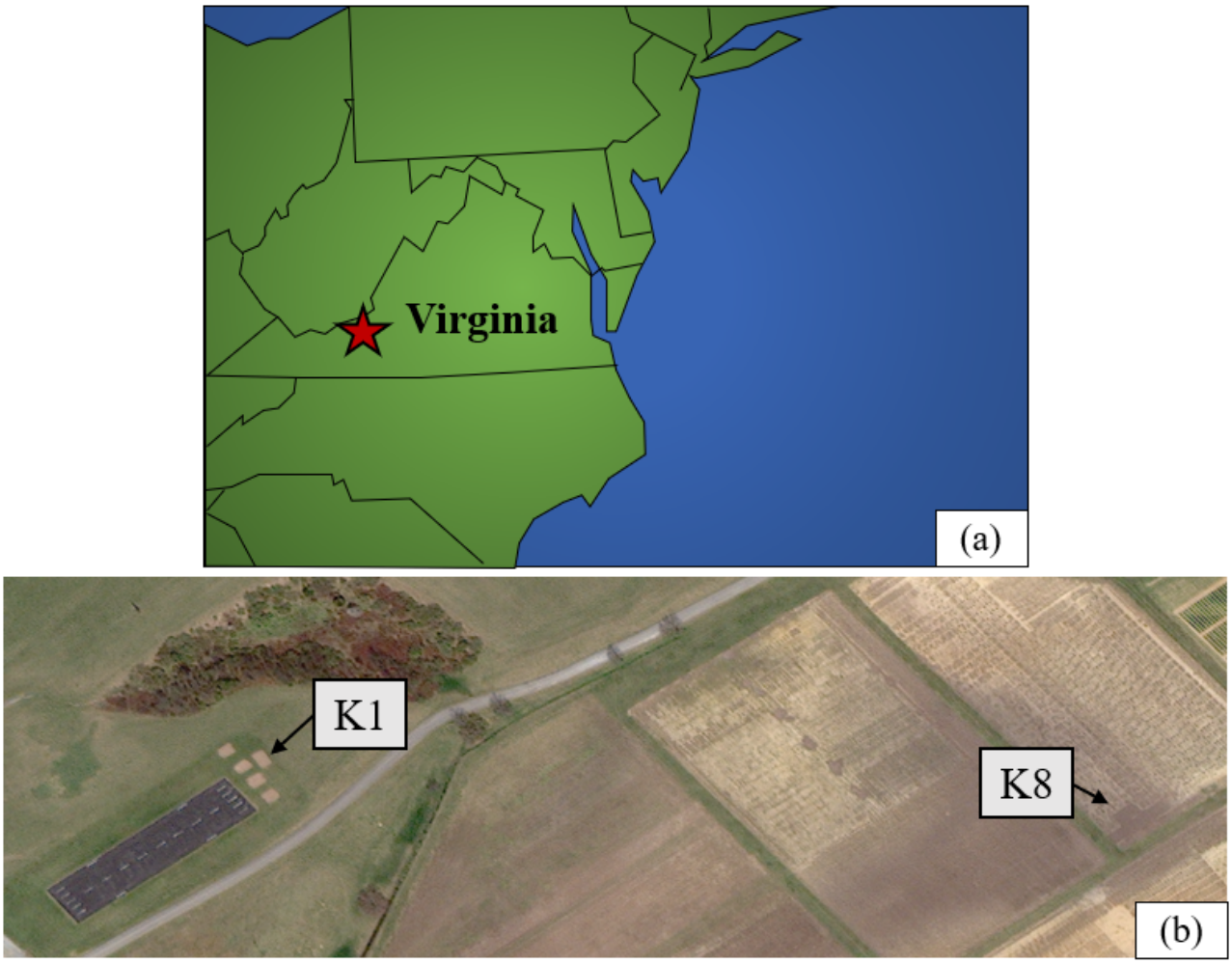

Figure 1. (a) Location of the Kentland Farm facility (red star) in Virginia in the Mid-Atlantic United States and (b) pansharpened image from 03 April 2019 at 16:12:22 UTC showing the location and layout of the soil patches.

Figure 2. Example of a multispectral image, showing band 7 of the image collected from the WorldView-2 satellite (NIR-1, 770-895 nm) on 03 April 2019 of Kentland Farm. The locations of sites K1 and K8 are labelled in the image.

Five patches (four 5.5 m by 5.5 m and one 7.3 m by 5.5 m) were prepared at each site to achieve different unit weights through plowing and compaction and moisture contents through irrigation. Vegetation was removed from the patches in order to maintain bare soils. The patches were situated on flat ground in order to limit effects from topography. Field measurements of moisture content, unit weight, shear strength, and erodibility were conducted from 17 March 2019 to 22 March 2019. During these measurements, soil samples were weighed and dried in an oven overnight to measure the natural moisture content. These measurements were made on the soil patches that were not disturbed by irrigation. Gravimetric moisture content measurements ranged from 11.8% and 26.0% with an average of 19.6% for site K1. For site K8, the gravimetric moisture contents ranged between 7.7% and 18.6% with an average of 16.5%. The higher in-situ moisture contents at K1 are likely a result of the vegetation in the area; K1 was situated in a grassy field while K8 was located in an empty field with significantly less vegetation nearby (see Fig.1b) [21]. A previous site investigation at Kentland Farm in August 1997 classified the surface soils as sandy lean clay and sandy silt with natural moisture contents ranging from approximately 18.0% to 22.0% [22].

The soil patches were not further disturbed or irrigated after the final measurements on the 22 March 2019, except for rainfall, allowing the moisture content to equilibrate in all five patches of each soil type. This would lead to similar moisture contents being estimated for each soil patch.

3. Methods

3.1. Long-term Sensors

Kentland Farm maintains sensors for monitoring soil conditions, with historical data available online at the Montgomery Country WeatherSTEM data mining tool for Virginia Tech Kentland Farm. Data records are available starting on 17 June 2016 and can be accessed in intervals of minutes, hours, days, or months [23]. Sensor measurements for total daily rainfall and average daily soil moisture tension at a depth of 15.2 cm for a three-week period starting on 16 March 2019 and ending on 04 April 2019 were compiled. Soil moisture tension is the energy needed to remove water from the soil [24]. These measurements were compiled in order to understand the ground conditions during satellite overflight and field measurements.

3.2. Spectral Signatures

Spectral signatures, also known as spectral response patterns, refer to the distinct pattern of reflectance of an object at different wavelengths. These patterns do not exhibit absolute values for a given object; instead, the patterns fall within a range for an object. This results in a range of reflectance values that can be used to characterize an object. For bare soils, the reflectance is impacted by moisture content, soil type, roughness, and organic content, which in turn impacts the spectral signature of a soil [17].

Spectral signatures of objects can be found through several means. The two primary methods used in agricultural and coastal engineering have been the use of either ground-based spectrometers or satellite-based multispectral imagery.

For this study, spectral signatures were collected in the laboratory using an ASD FieldSpec® Spectroradiometer with RS3 instrument control software. Reflectance of the soil samples are measured in the visible-near infrared (350 nm - 1050 nm) and short-wave infrared (1000 nm - 2500 nm) bands using three on-board spectrophotometers [25]. A single reflectance value was assigned to each wavelength. A directly lit high intensity contact probe was used to illuminate the samples and collect the spectral signatures.

Soil samples were dried overnight and broken down so minimal clods existed in the samples. Samples were then prepared to a range of moisture contents, ranging from zero to the liquid limit of each soil in intervals of 5% moisture content. Four spectra were collected for completely dry samples and two spectra were collected for samples prepared to each moisture content in order to account for the inherent variability in spectral signatures [17].

The raw reflectance values were processed in MATLAB® and plotted over the corresponding wavelengths to create the spectral signatures. The reflectance from each spectral signature was averaged over wavelengths corresponding to four bands in the electromagnetic spectrum: blue (450 nm - 510 nm), green (510 nm - 580 nm), red (630 nm - 690 nm), and NIR (770nm - 895 nm). The average reflectance for the NIR band for each corresponding moisture content were

plotted and fit with a best fit line in the form of Eq. (1). The coefficients of the best-fit line allow determined $a_{s(\lambda)}$ and $\rho_{so(\lambda)}$.

3.3. Satellite Imagery

A satellite-based multispectral image of Kentland Farm was collected on 03 April 2019. The image was obtained from the WorldView-2 satellite, which simultaneously collects data over eight regions of the electromagnetic spectrum: coastal (400 nm - 450 nm), blue, (450 nm - 510 nm), green (510 nm - 580 nm), yellow (585 nm - 625 nm), red (630 nm - 690 nm), red edge (705 nm - 745 nm), NIR-1 (770 nm - 895 nm), and NIR-2 (860 nm - 1040 nm) [26]. The image has a mean ground sampling distance of 2.1 meters per pixel. For this study, the reflectance values from the NIR-1 band were selected to estimate the in-situ moisture content, as the IR regions of the electromagnetic spectrum are more sensitive to changes in moisture content than the visible regions [13, 15]. Prior to image delivery, images were corrected for atmospheric and haze effects utilizing DigitalGlobe's Atmospheric Compensation algorithm [27]. Images were first corrected to top-of-atmosphere radiance and then reflectance [28].

The reflectance values for each pixel that fell into the respective soil patches were then extracted and used to calculate the average moisture content for each plot. Only pixels completely contained within the outline of the soil patches were used to eliminate boundary effects (i.e., mixed pixels where the reflectance values of different conditions are contained within a single pixel).

To solve for moisture content, Eq. (1) was rewritten into the following form:

$$m = \frac{\ln\left(\frac{\rho_{s(\lambda)}}{\rho_{so(\lambda)}}\right)}{-a_{s(\lambda)}} \quad (2)$$

Using the coefficients of a best-fit line in the form of Eq. (1) for $a_{s(\lambda)}$ and $\rho_{so(\lambda)}$ and the reflectance values extracted from the multispectral image, the moisture content of each pixel, and each soil patch, can be estimated.

The image in Fig. 2 shows the reflectance values from the NIR-1 band from the multispectral image collected on 03 April 2019 of Kentland Farm. It can be assumed that the reflectance value represents the average conditions over the entire 4.4 m^2 pixel.

4. Results and Discussion

4.1. Site Conditions

Figure 3 presents the total daily rainfall data from 16 March 2019 to 04 April 2019. Figure 4 displays the average daily soil moisture tension over the same date range. A higher soil moisture tension indicates that there is a lower moisture content. Both the daily rainfall data and average daily soil moisture tension indicate dry conditions at Kentland Farm during both field measurements and satellite overflight. During both field measurements and satellite image collection there was no rainfall recorded at the site. The maximum recorded rainfall over the three-week period was 0.1 cm on 25 March 2019. Thus, relatively low moisture contents are expected during the satellite overflight.

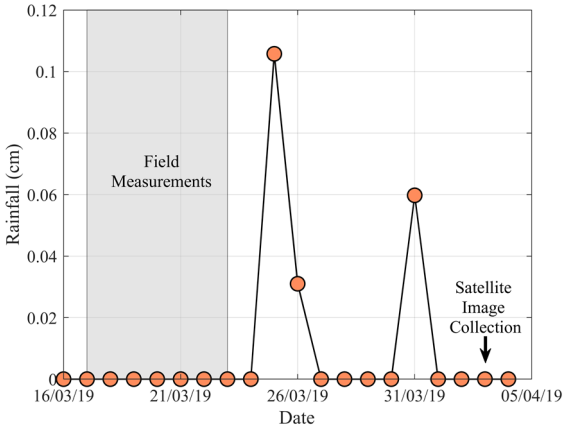

Figure 3. Total daily rainfall at the Kentland Farms weather station. Data was obtained from the Montgomery County WeatherSTEM data mining tool [23]. The dates of field measurements and satellite image collection are indicated by the grey shaded area and the arrow, respectively.

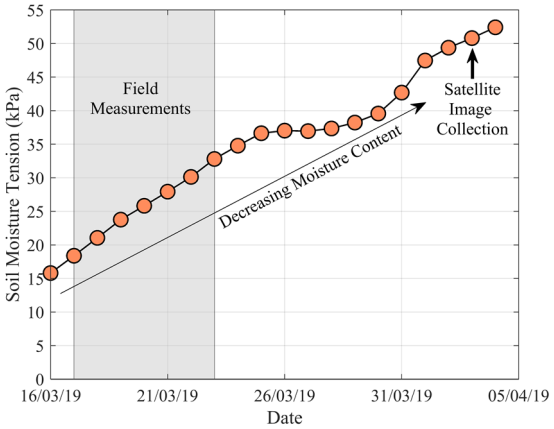

Figure 4. Average daily soil moisture tension at the Kentland Farms weather station. Data was obtained from the Montgomery County WeatherSTEM Data mining tool [23]. The dates of field measurements and satellite image collection are indicated by the grey shaded area and the arrow, respectively.

4.2. Spectral Signatures

The spectral signatures collected using the ASD FieldSpec® Spectroradiometer for soils found at sites K1 and K8 are presented in Figs. 5 and 6, respectively. The labels in each figure indicate the moisture content over which the soil samples were prepared, ranging from completely dry to the liquid limit for each soil, in intervals of 5% moisture content. The orange lines are the complete spectral signatures collected over the entire range of wavelengths and the purple lines are the averaged spectral signatures. The spectral signatures for K1 (Fig. 5) exhibit similar values of reflectance for low water contents (0.0%-5.0%); this is a result of difficulties in modeling the soil moisture-reflectance relationship at low water contents [11]. A decrease in the moisture content resulted in a decrease in the recorded reflectance for both soils, with a greater decrease in reflectance noted at lower moisture contents. The change in reflectance with increasing moisture content followed an exponential pattern as expected [9-16]. The reflectance saturated and

exhibited little change with increasing moisture content at a moisture content of approximately 25.0% for K1 and 20.0% for K8.

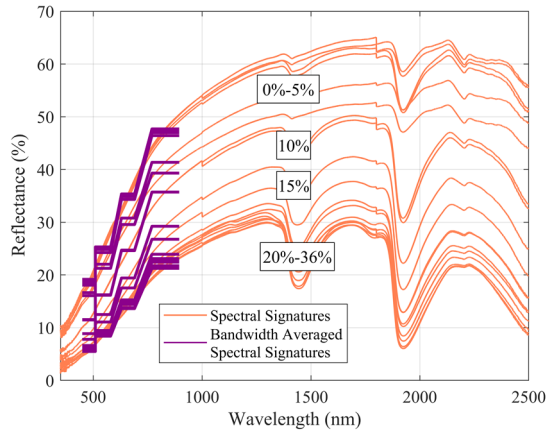

Figure 5. Spectral signatures collected from the ASD FieldSpec® Spectroradiometer for the soil at site K1. The orange lines represent the spectral signature of the soil prepared at moisture contents ranging from 0% to the liquid limit, with the labels indicating the moisture content of the respective signature. The purple lines represent the spectral signatures averaged over four bands of wavelengths from the WorldView-2 satellite. See text for details.

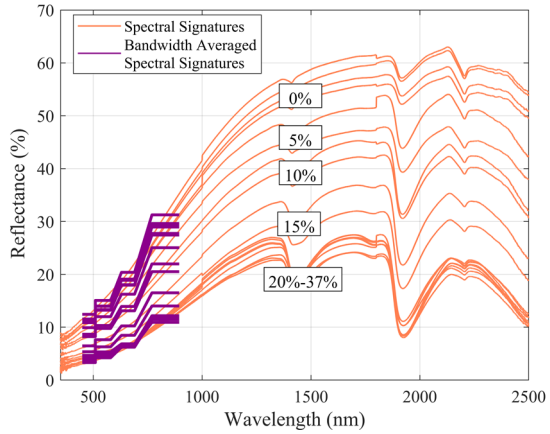

Figure 6. Spectral signatures collected from the ASD FieldSpec® Spectroradiometer for the soil at site K8. The orange lines represent the spectral signature of the soil prepared at moisture contents ranging from 0% to the liquid limit, with labels indicating the moisture content of the respective signature. The purple lines represent the spectral signatures averaged over four bands of wavelengths from the WorldView-2 satellite. See text for details.

Figure 7 shows the moisture content plotted against the averaged reflectance collected from the ASD FieldSpec® Spectroradiometer over the wavelengths that correspond to the NIR-1 band from the WorldView-2 satellite for the two soils. Soil from site K8 exhibits lower reflectance values than soil from site K1 as expected since the soil is darker in color (see Fig. 1b). The two lines represent best fit lines in the form of Eq. (1). The coefficients $a_{s(\lambda)}$ and $\rho_{so(\lambda)}$ are 0.0245 and 0.4562 for K1 and 0.0334 and 0.2938 for K8, respectively. The best-fit line for K1 and K8 achieve R^2 values of 0.86 and 0.93, respectively. For K1, there is more variability in the reflectance values at lower moisture contents (0% - 5%). Previous studies indicate that dry soils (less than approximately 10% moisture content) can display a greater range of reflectance measurements. These effects are also exacerbated by the presence of silt [10,11].

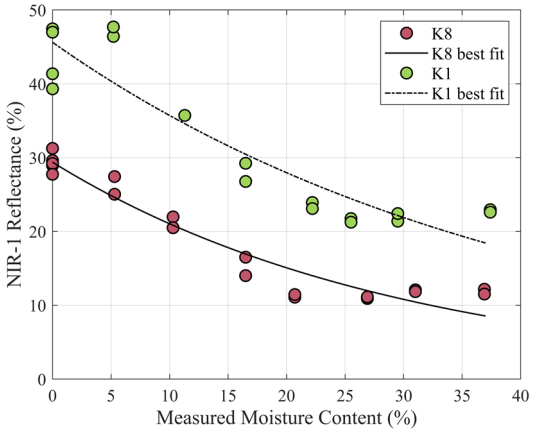

Figure 7. Averaged reflectance data from the spectral signatures over wavelengths corresponding the NIR-1 (770 nm - 895 nm) band of WorldView-2 imagery with best fit lines in the form of Eq. (1) to establish the parameters $a_{s(\lambda)}$ and $\rho_{so(\lambda)}$ for soils at sites K1 and K8.

4.3. Estimating Moisture Content from Satellite Imagery

The moisture content for each pixel was estimated using the reflectance values of pixels located in each soil patch of sites K1 and K8 from Fig. 2 with Eq. (2). Figure 8 presents the percentage of pixels that fall within each bin of estimated moisture content as compared to a normal distribution of estimated moisture contents for site K1. Even though it is assumed that all five patches are at a single moisture content, reflectance values (and moisture content estimates) will produce a distribution of values. This distribution is due to spatial variability in surface roughness and organic content combined with the inherent variability in spectral signatures [17]. Assuming a normal distribution, the estimated moisture contents from site K1 present a mean of 18.8% and a standard deviation of 2.3%.

The estimated moisture contents for site K1 do not follow a normal distribution. Muller and Décamps [11] indicate that Eq. (1) produces the worst fit for silts and silty clays; the soil at site K1 classifies as a sandy silt. Nevertheless, the mean estimated moisture content falls well within the range of moisture contents observed during both the August 1997 and March 2019 surveys.

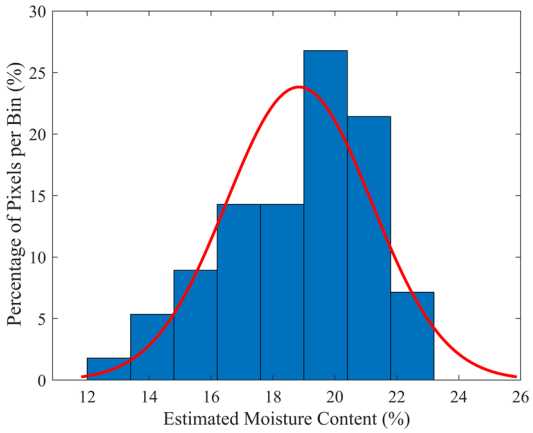

Figure 8. Percentage of pixels within each bin of estimated moisture content (blue boxes) compared to an assumed normal distribution (red line) for site K1. See text for details.

The mean estimated moisture content is on the lower end of the measured moisture contents during the two field surveys. From Fig. 4, it is shown that conditions are slightly drier than during the March 2019 measurements, leading to a slightly lower estimated moisture content.

Figure 9 presents the percentage of pixels that fall within each bin of estimated moisture content as compared to a normal distribution of estimated moisture contents for site K8. Here, the estimates of moisture content present a mean of 14.8%, a standard deviation of 1.7%, and fall within a normal distribution. The results of Muller and Décamps [11] indicate that Eq. (1) should produce reasonable results for clayey soils, leading to the normal distribution being reasonable for clayey soils.

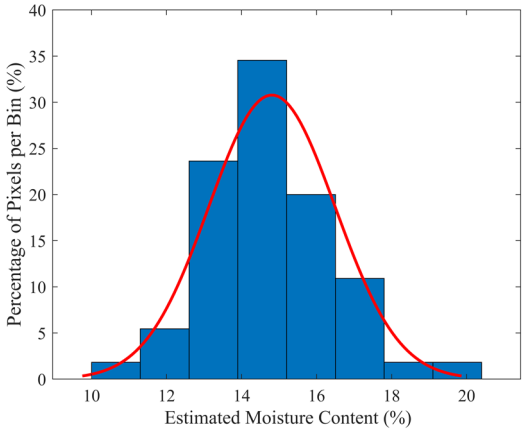

Figure 9. Percentage of pixels within each bin of estimated moisture content (blue boxes) compared to an assumed normal distribution (red line) for site K8. See text for details.

The range of estimated moisture contents observed at K8 are generally lower than those observed from measurements during the August 1997 survey but fall within the range of moisture contents observed in the March 2019 survey. Here, the lowest estimate of moisture content (10.2%) was higher than the lowest measured moisture content (7.7%) and the highest estimate is higher (19.9%) than compared to field measurements (18.6%); these differences are a result of the difficulties in modeling the reflectance-soil moisture relationship at low moisture contents as well as issues related to modeling the reflectance relationship of darker soils. These trends have been observed by others [10, 11]. The soils at K8 classified as a lean clay/silt and contained less than 10% sand while the soils observed in the 1997 survey classified as sandy clays and silts. A variability in soil type would impact the moisture content that is observed at the sites. Furthermore, the average moisture content during the March 2019 survey for site K8 was 16.5%. Similar to site K1, Fig. 4 indicates drier soil conditions during satellite overflight than during field measurements, leading to a slightly lower estimated moisture content from satellite imagery than observed during the March 2019 field measurements.

The engineering behavior of soils is greatly impacted by the water content of the soil. Holtz et al. [29] present three stress-strain curves to represent the behavior of the same soil at different water contents. From 0% water content to the plastic limit, the soil behaves as a brittle material. For water contents between the plastic limit and the liquid limit, the soil behaves as a plastic solid. Finally, at water contents beyond the liquid limit, the soil will behave as a viscous liquid. By identifying the regime that the range of moisture contents fall, the general behavior of the soil can be determined.

Kaleita et al. [10] suggest that Eq. (1) and the wavelengths over which multispectral satellites operate might be more effective in identifying moisture content regimes than precise measurements of moisture content. Depending on where the range of moisture contents fall, it would be possible to determine the behavior of the soil. For example, in this study the estimated moisture contents fell below the plastic limit, leading to the prediction that the soil would behave as a brittle solid. Theoretically, the relationship between moisture content and soil reflectance improves with increasing moisture content. These relationships could potentially be useful in identifying soils that are near and above their liquid limit, which would be the most problematic for engineering design.

When the water content of the soil falls between the plastic limit and the liquid limit, the behavior of the soil is highly variable. When the water content is close to the plastic limit, the behavior is ductile while when the water content is closer to the liquid limit the stress-strain behavior is more linear. Therefore, it becomes necessary to establish a more accurate estimate of moisture content. Increased accuracy can be established by using a higher resolution image. Synthetic aperture radar (SAR) systems, like TerraSAR-X, have the capability of offering a resolution of up to 0.25 meters [30]. During this study, SAR images were collected from 17 March 2019 to 22 March 2019. This allows for the opportunity to explore the idea of using multispectral images to establish general regimes of moisture content and SAR to establish a more refined assessment.

5. Conclusions and Future Work

A method for estimating the moisture content of bare, fine grained sediments was tested. In order to estimate moisture content, Eq. (2) was solved based on reflectance data extracted from a NIR band of a satellite-based multispectral image. The two other parameters needed to solve Eq. (2), $a_{s(\lambda)}$ and $\rho_{so(\lambda)}$, were found using spectral signatures of soils prepared to moisture contents ranging from 0% to the liquid limit of the soil. Two areas of the Kentland Farm at Virginia Tech with unique soil properties were tested. Five soil patches at each site were cleared of vegetation and prepared to various unit weights and moisture contents. Measurements of moisture content were carried out the week of 17 March 2019 to 22 March 2019. A satellite image of Kentland Farm was taken on 03 April 2019 using the WorldView-2 satellite. The results showed a good agreement between the field measurements and the estimated moisture content from the satellite image.

The overall goal of the project is to develop a methodology for assessing moisture content of coastal sediments in relation to beach trafficability from remote sensing. Optic remote sensing systems can only successfully operate in conditions of limited cloud coverage and at certain times of day. These systems are also limited by their resolution. Future work will focus

on developing and improving methods for assessing moisture content by other remote sensing technologies, such as SAR, which has the capability of operating in a range of weather conditions and times of day.

Acknowledgements

The authors acknowledge funding from the Office of Naval Research (ONR) through grants N00014-17-1-2516 and N00014-18-2435. The authors would also like to thank Matthew Florence, Reem Jaber, Dennis Kiptoo, Gaby Nolivos, Sam Consolvo, Nick Brilli, and Chris McBride for assistance with field measurements and laboratory testing as well as the technical staff at Kentland Farm for assistance with the selection and preparation of the soil patches.

References

[1] Lambe, T.W, Whitman, R.V. "Soil mechanics", 1st ed., John Wiley and Sons, New York, USA, 1969.

[2] Dean, R.G., Dalrymple, R.A. "Coastal processes with engineering applications", 1st ed., Cambridge University Press, New York, USA, 2004, https://doi.org/10.1017/CBO9780511754500.002

[3] Paprocki, J., Stark, N., McNinch, J. E., Wadman, H. "Spatial and temporal variations in moisture content at a sandy beach and the impact on sediment strength", In: 8th International Conference on Case Histories in Geotechnical Engineering, Philadelphia, USA, 2019, pp. 258-265. https://doi.org/10.1061/9780784482131.027

[4] Zhu Y. "Modeling Spatial and Temporal Variations of Surface Moisture Content and Groundwater Table Fluctuations on a Fine-grained Beach, Padre Island, Texas", PhD, Louisiana State University, 2007. [online] Available at: https://digitalcommons.lsu.edu/gradschool_dissertations/2613/ [Accessed: 07 June 2018].

[5] Jenkins, S. A. "Clandestine methods for the determination of beach trafficability, SIO reference #85-27", [pdf] University of California Scripps Institution of Oceanography, San Diego, USA, Available at: https://apps.dtic.mil/dtic/tr/fulltext/u2/a163007.pdf [Accessed: 18 August 2019].

[6] Mulhearn, P. J. "Methods for obtaining soil strength data for modelling vehicle trafficability on beaches: DSTO-DG-0299", [pdf] Defence Science and Technology Organisation, Victoria, AUS, Available at: https://apps.dtic.mil/dtic/tr/fulltext/u2/a395739.pdf [Accessed:18 August 2019].

[7] Wong, J. Y. "Terramechanics and off-rad vehicles", 1st ed., Elsevier, New York, USA, 1989.

[8] Stark, N., Paprocki, J., Brilli, N., McBride, C., Graber, H. C. "Rapid coastal sediment characterization from satellite imagery", In: 9th International Conference on Coastal Sediments 2019, Tampa/St. Petersburg, USA, 2019, pp. 2607-2620. https://doi.org/10.1142/9789811204487_0224

[9] Bowers, S. A., Hanks, R. J. "Reflection of radiant energy from soils", Soil Science, 100(2), pp. 130-138, 1965. [online] Available at: https://infosys.ars.usda.gov/WindErosion/publications/Andrew_pdf/870.pdf [Accessed 16 August 2019]

[10] Kaleita, A. L., Tian, L. F., Hirschi, M. C. "Relationship between soil moisture content and soil surface reflectance", Transactions of the ASAE, 48(5), pp. 1979-1986, 2005. https://doi.org/10.13031/2013.19990

[11] Muller, E., Décamps, H. "Modeling soil moisture-reflectance", Remote Sensing of Environment, 76(2), pp. 173-180, 2001. https://doi.org/10.1016/S0034-4257(00)00198-X

[12] Leu, D. J. "Visible and near-infrared reflectance of beach sands: a study on the spectral reflectance/grain size relationship", Remote Sensing of Environment, 6(3), pp. 169-182, 1977. https://doi.org/10.1016/0034-4257(77)90002-5

[13] Lobell, D. B., Asner, G. P. "Moisture effects on soil reflectance", Soil Science of America Journal, 66(3), pp. 722-727, 2002. https://doi.org/10.2136/sssaj2002.0722

[14] Paprocki, J., Stark, N., Graber, H. C., McNinch, J., Wadman, H. "Use of multispectral imagery for geotechnical characterization of sandy beach sediments", In: 9th International Conference on Coastal Sediments 2019, Tampa/St. Petersburg, USA, 2019, pp. 2553-2565. https://doi.org/10.1142/9789811204487_0220

[15] Shin, H., Yu, J., Jeong, Y., Wang, L, and Yang D. "Case-based regression models defining the relationships between moisture content and shortwave infrared reflectance of beach sands", IEEE Journal of Selected Topics in Applied Earth Observations and Remote Sensing, 10(10), pp. 4512-4521, 2017. https://doi.org/10.1109/JSTARS.2017.2723912

[16] Shuchman, R. A., Rea, D. K. "Determination of beach sand parameters using remotely sensed aircraft reflectance data", Remote Sensing of Environment, 11, pp. 295-310, 1981. https://doi.org/10.1016/0034-4257(81)90027-4

[17] Lillesand, T. M., Kiefer, R. W., Chipman, J. W. "Remote sensing and image interpretation", 7th ed., John Wiley and Sons, Inc., Hoboken, USA.

[18] Manning, M., Stark, N. "Investigating moisture contents of sandy beaches in the context of a geotechnical site characterization", In: 9th International Conference on Coastal Sediments 2019, Tampa/St. Petersburg, USA, 2019, pp. 2541-2552. https://doi.org/10.1142/9789811204487_0219

[19] ASTM "D2487-17 – Standard Practice for classification of soils for engineering purposes (unified soil classification system)", ASTM International, West Conshohocken, USA, 2018. https://doi.org/10.1520/D2487-17

[20] ASTM "D7928-17 – Standard test method for particle-size distribution (gradation) of fine-grained soils using the sedimentation (hydrometer) analysis", ASTM International, West Conshohocken, USA, 2018. https://doi.org/10.1520/D7928-17

[21] Francis, C F. Thornes, J. B., Romero Diaz, A., Lopez Bermudez, F., and Fisher, G.C. "Topographic control of soil moisture, vegetation cover and land degradation in a moisture stressed Mediterranean environment", Catena, 13(1-2), pp. 211-225, 1986. https://doi.org/10.1016/S0341-8162(86)80014-5

[22] Mokwa, R. L. "Investigation of the resistance of pile caps to lateral loading", PhD, Virginia Polytechnic Institute and State University, 1999.

[23] WeatherSTEM "Data mining", [online] Available at: https://montgomery.weatherstem.com/data?refer=/kentlandfarm [Accessed: 27 July 2019].

[24] Merriam-Webster "soil-moisture tension", [online] Available at: https://www.merriam-webster.com/dictionary/soil-moisture%20tension [Accessed: 18 February 2020].

[25] ASD "FieldSpec® user's guide" Analytical Spectral Devices, Inc., Boulder, USA, 1999.

[26] DigitalGlobe, "WorldView-2 data sheet", [pdf] DigitalGlobe, Available at: https://dgv4-cms-production.s3.amazonaws.com/uploads/document/file/130/WorldView2-DS-WV2-rev2.pdf [Accessed: 19 August 2019].

[27] Pacifici, F. Longbotham, N., Emery, W. J. "The importance of physical quantities for the analysis of multitemporal and multiangular optical very high spatial resolution images", IEEE Transactions on Geoscience and Remote Sensing, 52(10), pp. 6241-6256, 2014. https://doi.org/ 10.1109/TGRS.2013.2295819

[28] Updike, T., Comp, C. "Radiometric use of WorldView-2", [pdf] DigitalGlobe, Available at: https://dg-cms-uploads-production.s3.amazonaws.com/uploads/document/file/104/Radiometric_Use_of_WorldView-2_Imagery.pdf [Accessed: 17 August 2019].

[29] Holtz, R. D., Kovacs, W. D., Sheahan, T. C. "An introduction to geotechnical engineering", 2nd ed., Pearson, Upper Saddle River, USA, 2011.

[30] Fritz, T., Eineder, M. "TerraSAR-X, ground segment, basic product specification document", [pdf] DLR, Available at: https://www.intelligence-airbusds.com/files/pmedia/public/r466_9_tx-gs-dd-3302_basic-product-specification-document_1_9.pdf [Accessed: 18 August 2019]